LCC-0063
May 2001

Linear Collider Collaboration Tech Notes

Varying alpha/lambda in NLC Structures — BNS Damping and Emittance Growth

G. Stupakov and Z. Li

Stanford Linear Accelerator Center
Stanford, CA

Abstract: In this note we consider the effect of varying this iris opening in the NLC structures on the beam dynamics and the rf efficiency in the linac.

Varying a/λ in NLC structures – BNS damping and emittance growth

G. Stupakov and Z. Li

SLAC, Stanford University, Stanford, CA 94309

In this note we consider the effect of the varying the iris opening a in the NLC structures on the beam dynamics and the RF efficiency in the linac.

The most important consequence of the variation of the iris openings is the change of the longitudinal and transverse wakefields. Wake as a function of parameter a for the NLC structures has been previously calculated by K. Bane. Here we will use his result for the scalings of the longitudinal wake w_l and transverse wake w_t with the geometrical dimensions of the structure:

$$\begin{aligned} w_l(s) &= \frac{Z_0 c}{\pi a^2} e^{-\sqrt{s/s_0}}, \\ \frac{dw_t(s)}{ds} &= \frac{2Z_0 c}{\pi a^4} e^{-\sqrt{s/s_1}}, \end{aligned} \tag{1}$$

where for the scaling parameters s_0 and s_1 we have

$$s_0 = 0.41 \frac{a^{1.8} g^{1.6}}{L^{2.4}}, \qquad s_1 = (a[\mathrm{m}])^{1.96}, \tag{2}$$

with g being the distance between the irises (gap) and L – the cell period (equal to the gap plus the iris thickness). The above formulas were derived assuming $2\pi/3$ phase advance between the structure cells.

The wakefields were calculated assuming $g = 7.09$ mm and $L = 8.75$ mm and four different ratios of $a/\lambda = 0.18$, 0.17, 0.16, 0.15 ($\lambda = 2.62$ cm corresponding to the frequency 11.424 GHz). The plots of the longitudinal and transverse wakes are shown in Fig. 1 and 2.

The beams dynamics in the NLC lattice (linac.cd1.1.trans) was simulated using the LIAR code for the nominal case with the following parameters: initial beam energy – 10 GeV, final beam energy – 500 GeV, number of particles in the bunch – 10^{10}, normalized vertical beam emittance at the entrance to the linac – $3 \cdot 10^{-8}$ m, and the rms bunch length – 150 μm.

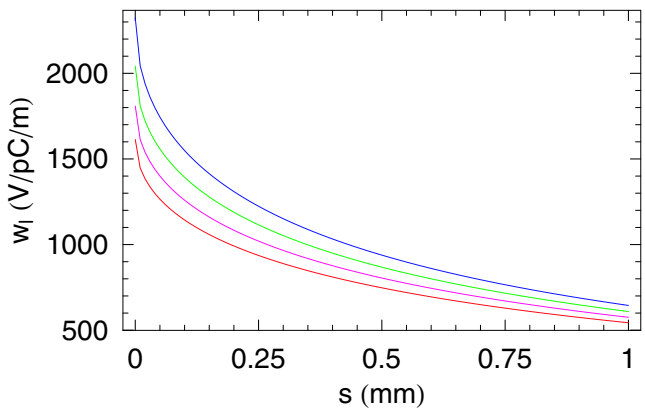

Figure 1: Longitudinal wake for four different values of a/λ: 0.15, 0.16, 0.17 and 0.18. The wake increases with the decrease of the ratio a/λ.

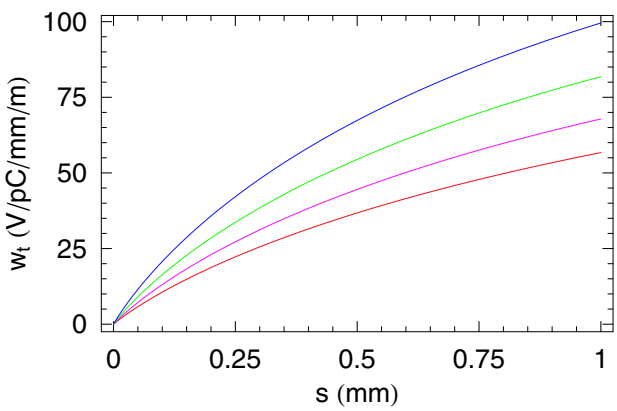

Figure 2: Transverse wake for four different values of a/λ: 0.15, 0.16, 0.17 and 0.18. The wake increases with the decrease of the ratio a/λ.

1 Case a/λ=0.18

Here we show the results of the simulations for the nominal NLC case $a/\lambda = 0.18$. The simulations were performed for 6 different energy spread profiles of the bunch (BNS regimes), see Fig. 3. The RF phases in the linac used for generation of the proper energy spread in each regime are listed in Table 1. Only a single bunch was simulated, and long-range wakefield effects were neglected.

Table 1: RF phases for different BNS regimes for a/λ=0.18.

Regime #	ϕ_1 [deg.]	E_1 [GeV]	ϕ_2 [deg.]	E_2 [GeV]	ϕ_3 [deg.]
1	4	30	-7	445.3	-30
2	8	30	-5	407	-30
3	10	30	-3	380	-30
4	12	30	-1	355	-30
5	14	30	1	331	-30
6	16	30	3	311	-30

Fig. 4 shows the emittance growth of the beam for an initial beam offset in the vertical direction 3.8 μm (equal to the vertical rms size of the beam at the entrance to the linac). In this figure the emittance is calculated relative to the centroid of the beam, and Fig. 5 shows the same simulation with the emittance calculated relative to the axis of the linac.

Fig 6 shows the emittance growth for the case when all structures in the linac are randomly misaligned with rms offset of 4 μm (the quadrupoles are perfectly aligned in this case). The plot represents an average over 100 random seeds.

As we see from Fig. 3 - 7, using the BNS regime 3 or higher practically suppresses the beam breakup instability in the linac.

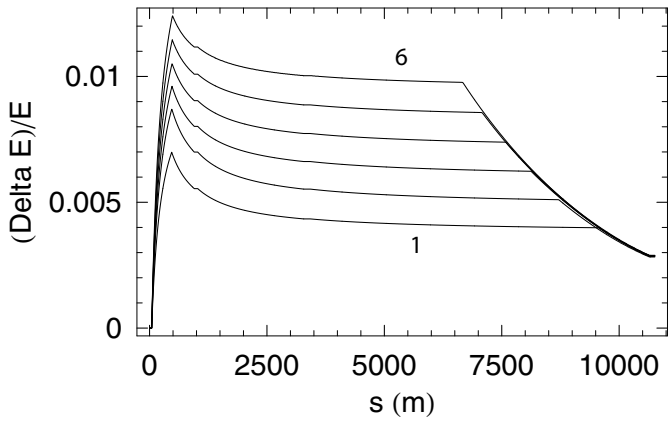

Figure 3: The correlated rms energy spread in the bunch as a function of position in the linac for different BNS regimes for $a/\lambda = 0.18$. The regime number increases from bottom to the top.

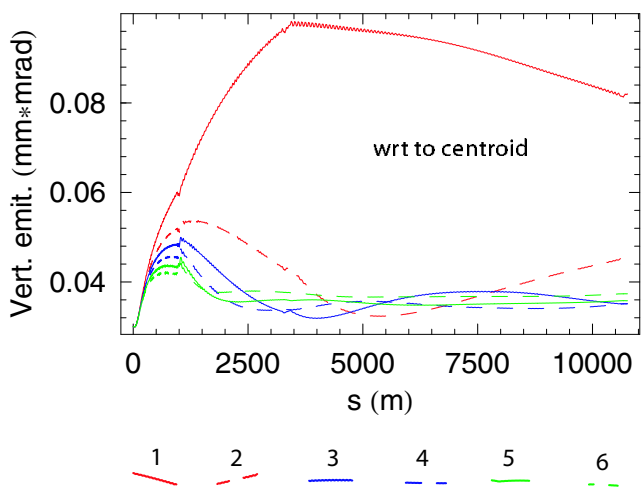

Figure 4: Beam emittance growth for initial offset of 1 σ_y for different BNS regimes for $a/\lambda = 0.18$. The emittance is measured with respect to the centroid of the beam. The color/dashing scheme showing correspondence to the BNS regime number is shown under the picture. This coloring is used consistently throughout the paper.

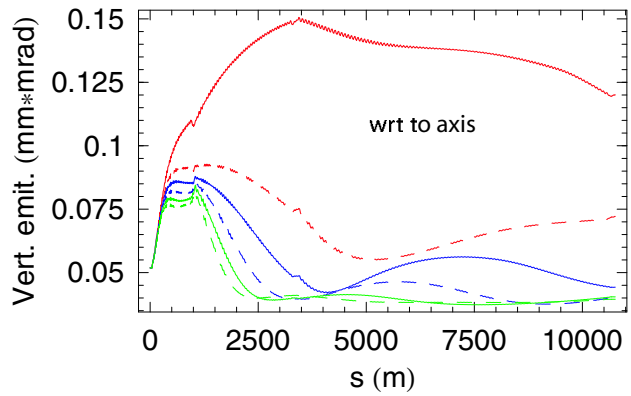

Figure 5: Beam emittance growth for initial offset of 1 σ_y for different BNS regimes for $a/\lambda = 0.18$. The emittance is measured with respect to the axis of the linac.

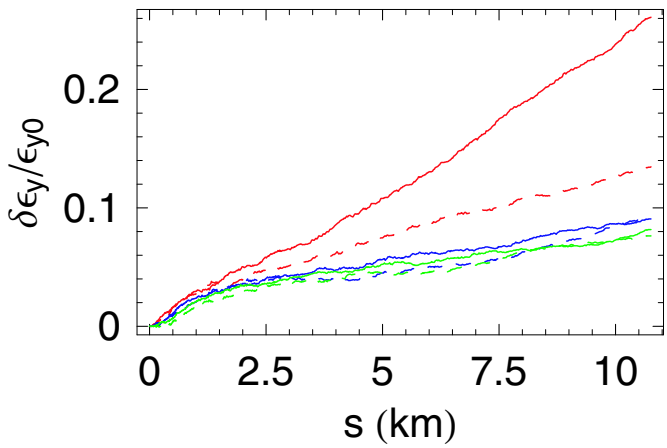

Figure 6: Beam emittance growth for random misalignment of structures for different BNS regimes for $a/\lambda = 0.18$. The rms structure offset is equal to 4 μm.

2 Case a/λ=0.17

In this section we present the results of the simulations for $a/\lambda = 0.17$. The 6 different energy spread profiles of the bunch (BNS regimes) are shown in Fig. 7. The RF phases in the linac used for generation of the energy spread in each regime are listed in Table 2.

Table 2: RF phases for different BNS regimes for a/λ=0.17.

Regime #	ϕ_1 [deg.]	E_1 [GeV]	ϕ_2 [deg.]	E_2 [GeV]	ϕ_3 [deg.]
1	4	30	-7	410	-30
2	7	30	-5	380	-30
3	10	30	-2	340	-30
4	13	30	1	310	-30
5	16	30	4	280	-30
6	19	30	7	260	-30

Fig. 8 shows the emittance growth of the beam for an initial beam offset in the vertical direction equal to 3.8 μm. In this figure the emittance is calculated relative to the centroid of the beam. Fig. 9 shows the same simulation with the emittance calculated relative to the axis of the linac. Fig. 10 shows the emittance growth for the case when all structures in the linac are randomly misaligned with rms offset of 4 μm. The plot represents an average over 100 random seeds.

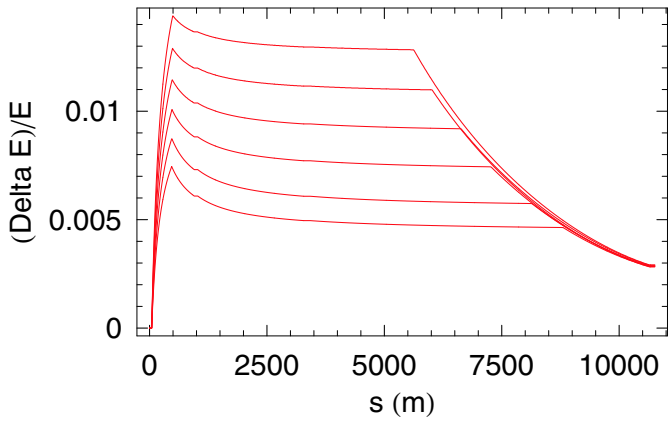

Figure 7: The correlated rms energy spread in the bunch as a function of position in the linac for different BNS regimes for $a/\lambda = 0.17$.

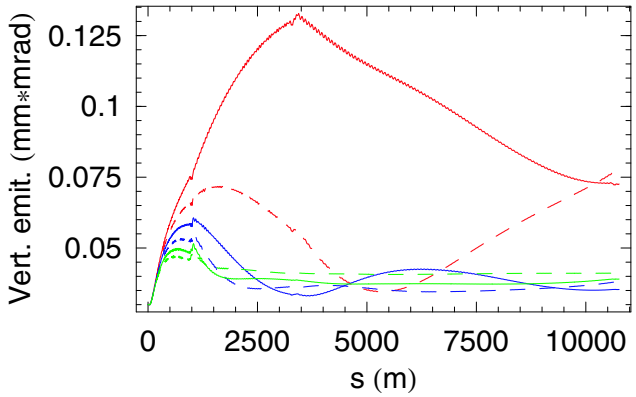

Figure 8: Beam emittance growth for initial offset of 1 σ_y for different BNS regimes for $a/\lambda = 0.17$. The emittance is measured with respect to the centroid of the beam.

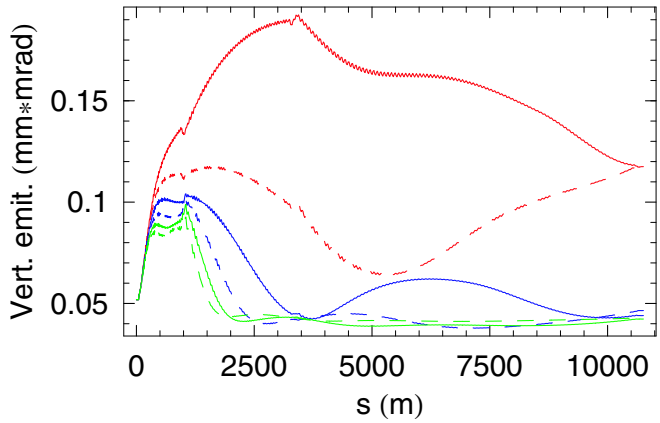

Figure 9: Beam emittance growth for initial offset of 1 σ_y for different BNS regimes for $a/\lambda = 0.17$. The emittance is measured with respect to the axis of the linac.

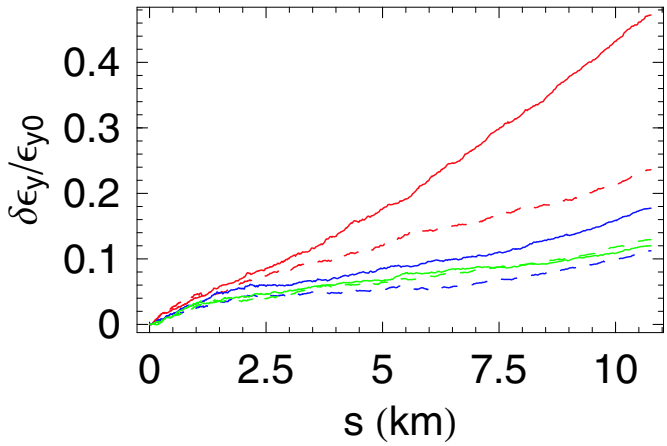

Figure 10: Beam emittance growth for random misalignment of structures for different BNS regimes for $a/\lambda = 0.17$. The rms structure offset is equal to 4 μm.

3 Case a/λ=0.16

In this section we present the results of the simulations for $a/\lambda = 0.16$. The 6 different energy spread profiles of the bunch (BNS regimes) are shown in Fig. 11. The RF phases in the linac used for generation of the energy spread in each regime are listed in Table 3.

Table 3: RF phases for different BNS regimes for a/λ=0.16.

Regime #	ϕ_1 [deg.]	E_1 [GeV]	ϕ_2 [deg.]	E_2 [GeV]	ϕ_3 [deg.]
1	3	30	-7	360	-30
2	6	30	-5	330	-30
3	9	30	-3	300	-30
4	12	30	-1	280	-30
5	15	30	1	260	-30
6	18	30	3	240	-30

Fig. 12 shows the emittance growth of the beam for an initial beam offset in the vertical direction equal to 3.8 μm. In this figure the emittance is calculated relative to the centroid of the beam. Fig. 13 shows the same simulation with the emittance calculated relative to the axis of the linac. Fig. 14 shows the emittance growth for the case when all structures in the linac are randomly misaligned with rms offset of 4 μm. The plot represents an average over 100 random seeds.

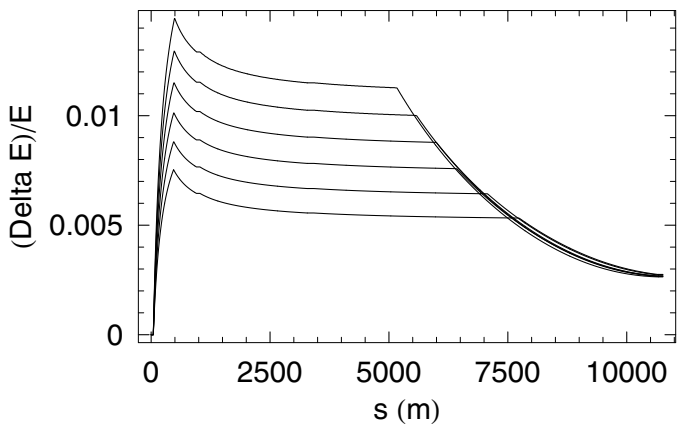

Figure 11: Energy spread in the bunch as a function of position in the linac for different BNS regimes for $a/\lambda = 0.16$.

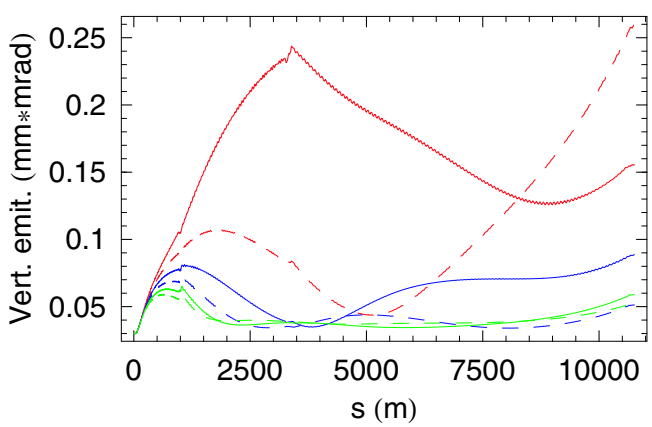

Figure 12: Beam emittance growth for initial offset of 1 σ_y for different BNS regimes for $a/\lambda = 0.16$. The emittance is measured with respect to the centroid of the beam.

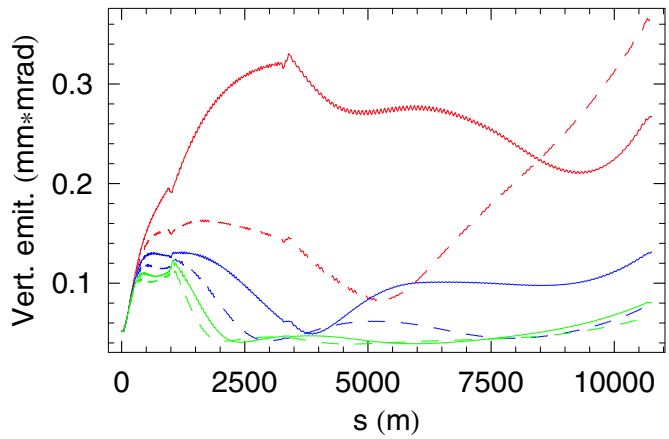

Figure 13: Beam emittance growth for initial offset of 1 σ_y for different BNS regimes for $a/\lambda = 0.16$. The emittance is measured with respect to the axis of the linac.

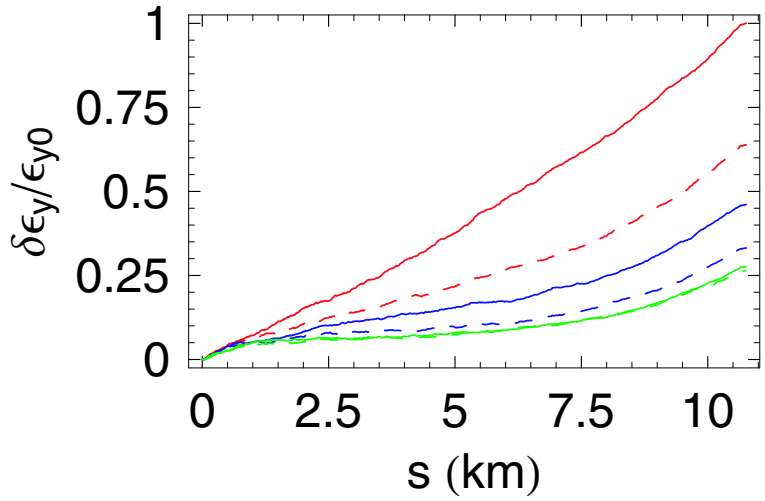

Figure 14: Beam emittance growth for random misalignment of structures for different BNS regimes for $a/\lambda = 0.16$. The rms structure offset is equal to 4 μm.

4 Case a/λ=0.15

The 6 different energy spread profiles of the bunch (BNS regimes) are shown in Fig. 15. The RF phases in the linac used for generation of the energy spread in each regime are listed in Table 4.

Table 4: RF phases for different BNS regimes for a/λ=0.15.

Regime #	ϕ_1 [deg.]	E_1 [GeV]	ϕ_2 [deg.]	E_2 [GeV]	ϕ_3 [deg.]
1	2	30	-7	320	-30
2	5	30	-5	290	-30
3	7	30	-3	270	-30
4	10	30	-1	250	-30
5	13	30	1	230	-30
6	16	30	3	220	-30

Fig. 16 shows the emittance growth of the beam for an initial beam offset in the vertical direction equal to 3.8 μm. In this figure the emittance is calculated relative to the centroid of the beam. Fig. 17 shows the same simulation with the emittance calculated relative to the axis of the linac. Fig. 18 shows the emittance growth for the case when all structures in the linac are randomly misaligned with rms offset of 4 μm. The plot represents an average over 100 random seeds.

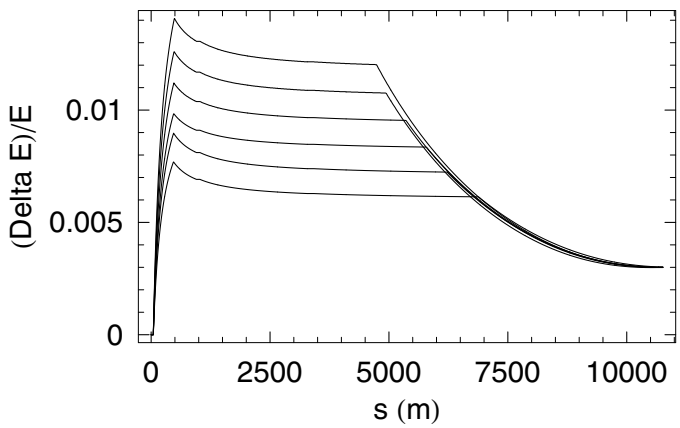

Figure 15: Energy spread in the bunch as a function of position in the linac for different BNS regimes for $a/\lambda = 0.15$.

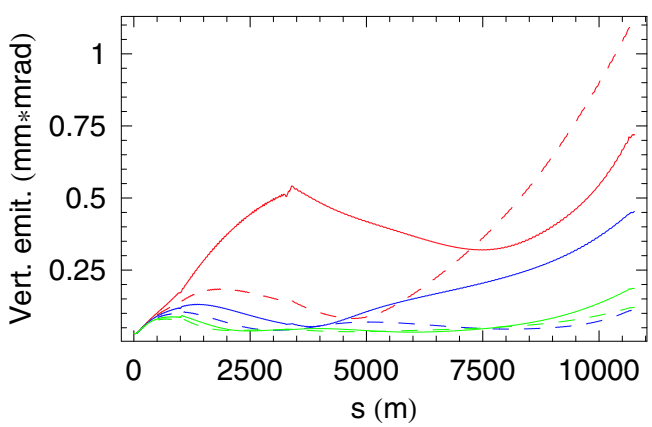

Figure 16: Beam emittance growth for initial offset of 1 σ_y for different BNS regimes for $a/\lambda = 0.15$. The emittance is measured with respect to the centroid of the beam.

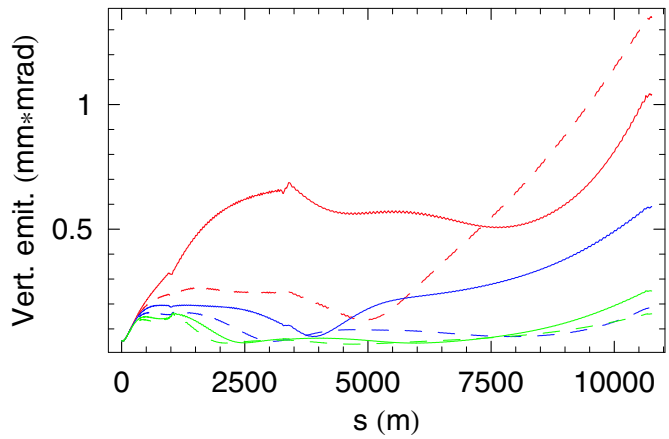

Figure 17: Beam emittance growth for initial offset of 1 σ_y for different BNS regimes for $a/\lambda = 0.15$. The emittance is measured with respect to the axis of the linac.

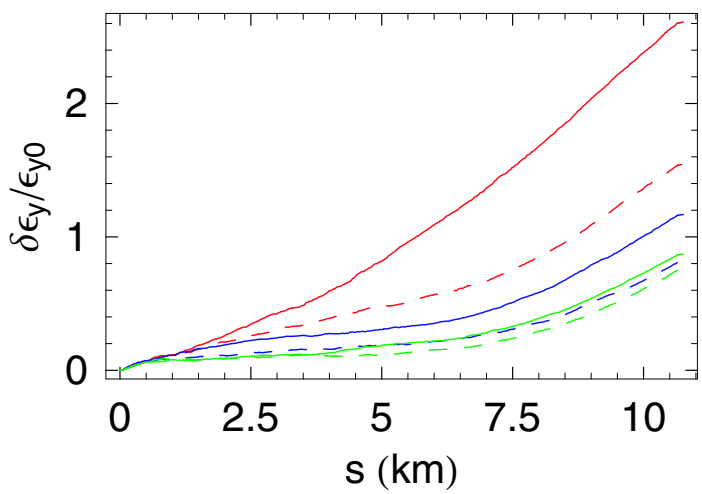

Figure 18: Beam emittance growth for random misalignment of structures for different BNS regimes for $a/\lambda = 0.15$. The rms structure offset is equal to 4 μm.

5 RF efficiency

In this section, we study the RF requirements for structures of different a/λ. We will use the LIAR lattice as the linac configuration. We will compare two types of structures with $a/\lambda = 0.18$ and 0.17 respectively. These structures are 90 cm in length. Both structures have a group velocity at the input-end of 3% of the speed of light and a filling time of about 120 ns. It is worthwhile to mention that in the LIAR lattice, the structures were assumed to be 180 cm in length, which is twice the length as we used here. The LIAR lattice is still valid if one substitutes the 180 cm structure with two 90 cm structures. We will pick the damping schemes #3 and #4 (see Tables 1 and 2) as our BNS damping models in these studies.

In the RF structure heavily loaded by a beam, the average gradient of the input RF, the beam loading, and the loaded can be represented by the diagram shown in Fig. 19, where ϕ_L corresponds to the BNS damping phase,

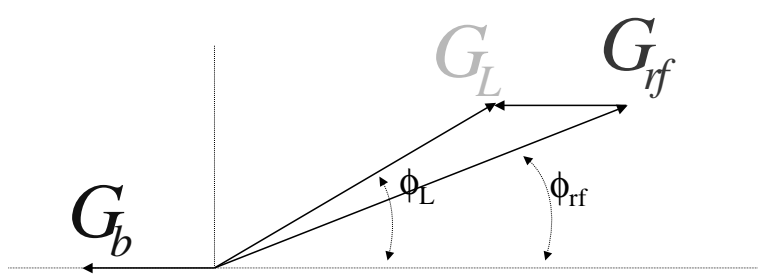

Figure 19: Average gradient in an accelerator structure with beam accelerated off crest. The ϕ_L is the BNS damping phase.

$\phi_{\rm rf}$ is the phase of the input RF relative to the beam. For the nominal beam of 1.1×10^{10} in bunch charge and 0.63 A in current, the single bunch loss factor and the long-range beam loading parameters for these two structures are as showing in Table 5.

Table 5: Beam loading parameters for a/λ=0.18 and 0.17.

	$a/\lambda = 0.18$	$a/\lambda = 0.17$
Single bunch (MV/m)	-0.869	-0.955
Long-range loading (MV/m)	-10.78	-11.45

We consider two operation scenarios:

1) Constant loaded gradient G_L along the linac, which is the assumption in the LIAR simulation. In this scenario, the input RF power of the structure needs to be adjusted in each of the BNS sections to compensate the differences in BNS phases. In reality, the maximum available RF power is limited by the klystron output.

2) Constant input RF power along the linac, e.g. constant unloaded gradient. The klystrons are assumed to run at full saturation. In this case, we will adjust the RF phases in each of the BNS sections such that the BNS slope "$G_L \sin(\phi_L)$" of the acceleration field is maintained. The assumption is that the LIAR lattice and BNS schemes are still valid. Admmitably, a consistent study of this scenario is needed in the future.

5.1 Scenario 1: Constant loaded gradient G_L

Given the loaded gradient G_L and BNS phase ϕ_L, the requirement on the gradient and the phase of the input RF can be calculated as the following

$$G_{\rm rf} = \sqrt{G_b^2 + G_L^2 - 2G_b G_L \cos(\phi_L)} + K_{loss},$$
$$\phi_{\rm rf} = \cos^{-1}\left(\frac{-G_b + G_L \cos(\phi_L)}{G_{\rm rf}}\right), \tag{3}$$

where K_{loss} is the single bunch loss factor. The effective linac length and the peak RF power needed for BNS section i are

$$z_i = \frac{\Delta E_i}{G_L \cos(\phi_i) - K_{loss}},$$

$$P_{peak,i} = z_i \left(\frac{G_{rf,i}}{G_{acc}} \right)^2 , \tag{4}$$

where G_{acc} is the RF gradient per unit input power per meter. The stored energy in the RF pulse is $U = P_{peak,i} \times T_{pulse}$, with $T_{pulse} = t_{fill} + T_b + T_{rise}$ the pulse length.

With the BNS parameters given in schemes #3 and #4, the RF power and linac length requirements for $a/\lambda = 0.18$ and 0.17 are obtained as shown in Figs. 20 and 21.

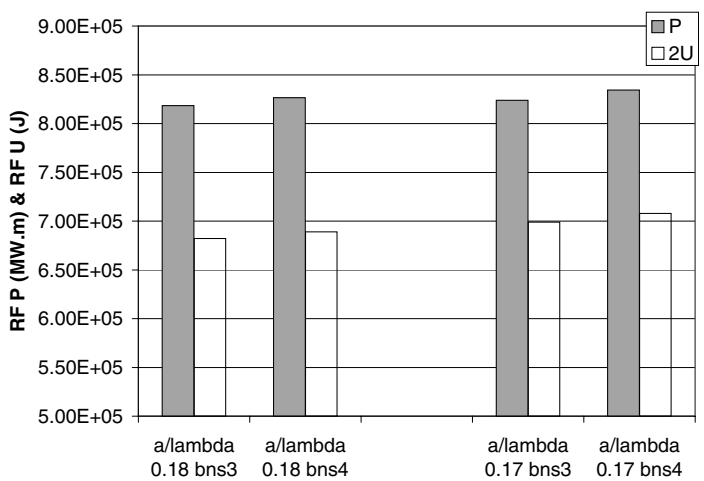

Figure 20: Peak RF power P and stored energy U for $a/\lambda = 0.18$ and 0.17 with BNS schemes #3 and #4. The energy is ploted in $2U$ for proper scaling.

5.2 Scenario 2: Constant unloaded $G_{\rm rf}$

With constant input power, the unloaded gradient is constant along the linac. In this case, we adjust the RF phase such that the slope of the acceleration is the same as in the LIAR lattice. The phase of the loaded gradient, however, will be different from the LIAR lattice due to changing in loaded gradient from BNS section to BNS section. Assuming A be the BNS slope in section i ("$A = G_L \sin(\phi_L)$"), the input and the loaded RF parameters are

$$G_{\rm rf} = G_{acc}\sqrt{P_{\rm rf}}, \qquad \phi_{\rm rf} = \sin^{-1}\left(\frac{A}{G_{\rm rf}}\right),$$

$$G_L = \sqrt{G_{\rm rf}^2 + G_b^2 + 2G_{\rm rf}G_b\cos(\phi_{\rm rf})}, \quad \phi_L = \sin^{-1}\left(\frac{A}{G_L}\right),$$

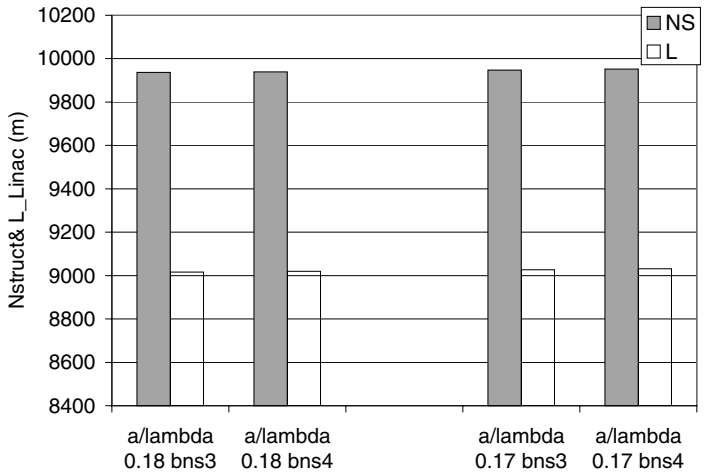

Figure 21: Linac length L and number of structure NS for $a/\lambda = 0.18$ and 0.17 with BNS schemes #3 and #4.

The power and length requirements for the linacs can be calculated using Eq.4.

In Figs. 22 and 23 are shown the comparison of the RF power and linac length for $a/\lambda = 0.18$ and 0.17 for the two BNS schemes.

5.3 Summary of RF comparison

With the same input power, the unloaded gradient of the structure is higher for the design with a smaller a/λ. However, the effective loaded gradient for smaller a/λ is offset by the larger average BNS phase and heavier beam loading. There is no gain in either RF power/energy requirement and linac length to reduce the a/λ from the nominal design of $a/\lambda = 0.18$. These simulations also suggest that in the structure design of heavily loaded linacs, one needs to take the optimization of the whole linac into account in addition to the single structure optimization.

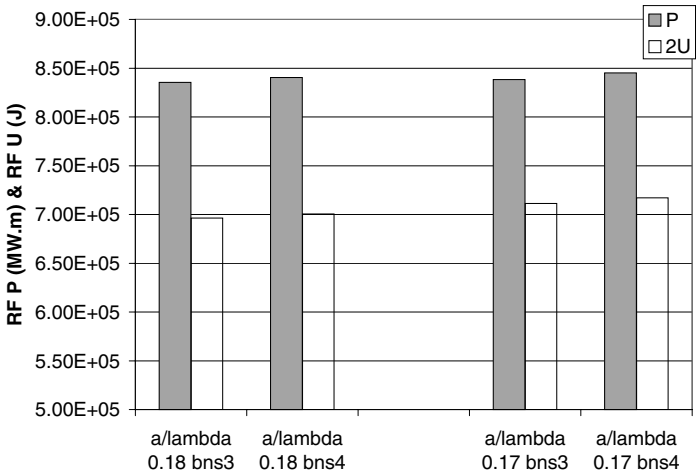

Figure 22: Peak RF power P and stored energy U for $a/\lambda = 0.18$ and 0.17 with BNS schemes #3 and #4. The energy is plotted in $2U$ for proper scaling.

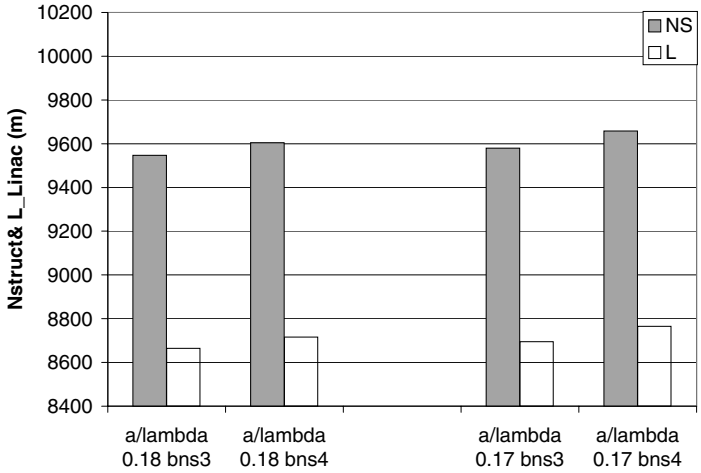

Figure 23: Linac length L and number of structure NS for $a/\lambda = 0.18$ and 0.17 with BNS schemes #3 and #4.